1 **Optimum stochastic modelling for GNSS tropospheric delay estimation in real-time**

2

3 Tomasz Hadas[1], Felix Norman Teferle[2], Kamil Kazmierski[1], Pawel Hordyniec[1], Jaroslaw

4 Bosy[1]

5

6 1) Institute of Geodesy and Geoinformatics, Wroclaw University of Environmental and Life

7 Sciences, Grunwaldzka 53, 50-357 Wroclaw, Poland

8 2) Geophysics Laboratory, University of Luxembourg, 6, rue Richard Coudenhove-Kalergi,

9 L-1359 Luxembourg, Luxembourg

10 tomasz.hadas@igig.up.wroc.pl, +48 713205617, fax. +48 713205617

11

12

13 **Abstract** In GNSS data processing the station height, receiver clock and tropospheric delay

14 (ZTD) are highly correlated to each other. Although the zenith hydrostatic delay (ZHD) of

15 the troposphere can be provided with sufficient accuracy, zenith wet delay (ZWD) has to be

16 estimated, which is usually done in a random walk process. Since ZWD temporal variation

17 depends on the water vapor content in the atmosphere, it seems to be reasonable that ZWD

18 constraints in GNSS processing should be geographically and/or time dependent. We propose

19 to take benefit from numerical weather prediction models to define optimum random walk

20 process noise. In the first approach we used archived VMF1-G data to calculate a grid of

21 yearly and monthly means of the difference of ZWD between two consecutive epochs

22 divided by the root square of the time lapsed, which can be considered as a random walk

23 process noise. Alternatively, we used the Global Forecast System (GFS) model from National

24 Centres for Environmental Prediction (NCEP) to calculate random walk process noise

25 dynamically in real-time. We performed two representative experimental campaigns with 20

26 globally distributed IGS stations and compared real-time ZTD estimates with the official

27 ZTD product from the International GNSS Service (IGS). With both our approaches, we

28 obtained an improvement of up to 10% in accuracy of the ZTD estimates compared to any

29 uniformly fixed random walk process noise applied for all stations.

30

---

33 _____

34 **Introduction**

35 Troposphere is a major error source in Global Navigation Satellite Systems (GNSS) precise

36 positioning, as the GNSS signal delay depends on the pressure, temperature and water vapor

37 content along the signal path. Furthermore, the delay can be divided into a hydrostatic and a

38 wet component (Mendes 1999). Hydrostatic delay of sufficient accuracy can be provided

39 with empirical models. Such models can be generally divided into two groups. The first

40 group requires surface meteorological data as an input and is based on empirical formula

41 proposed e.g. by Saastamoinen (1972) and Hopfield (1969), to provide tropospheric delay in

42 zenith direction (ZTD). The second group requires time and approximate coordinates to use

43 average parameters from numerical weather prediction (NWP) models e.g. GPT2 (Lagler et

44 al. 2013), UNB3 (Leandro et al. 2006). Unfortunately, wet delay depends on the water vapor

45 content, that changes rapidly over time and space. There is no model accurate enough for wet

46 delay, therefore wet delay is usually estimated as an unknown parameter. The wet delays for

47 each GNSS signal in slant direction are mapped into zenith direction using a mapping

48 function e.g. Niell (1996), UNB3, VMF1 (Böhm et al. 2009). In this way, an epoch-specific

49 parameter ZWD (zenith wet delay) is estimated in the functional model together with other

50 unknown parameters, including receiver coordinates and receiver clock error.

51 Although ZWD is treated as an error source in precise positioning, there is great

52 potential of exploiting ZWD for weather and climate monitoring (Bianchi et al. 2016,

53 Guerova et al. 2016). The very dense network of GNSS receivers distributed worldwide

54 becomes a powerful tool for remote sensing of water vapor in the troposphere, called GNSS

55 meteorology (Bevis et al. 1992). Compared to other existing techniques for water vapor

56 monitoring like water vapor radiometers or balloon radio-sounding, GNSS meteorology

57 operates in all weather conditions and provides homogenous products of spatial and temporal

58 resolution higher than any other tropospheric sensing technique (Vedel et al. 2001,

59 Hernandez-Pajares et al. 2001). It has already been demonstrated, that post-processing of

60 GNSS observations could provide results of accuracy comparable to the measurements of

61 traditional PWV sensors (Pacione and Vespe 2008, Satirapod et al. 2011). ZWD derived from

62 GNSS can be assimilated into NWP models in order to improve forecasting, especially during

63 severe weather conditions (Bennit and Jupp 2012, Karabatic et al. 2011, Rohm et al. 2014).

64 This was already investigated during EU COST Action 716
65 (http://www.cost.eu/COST_Actions/essem/716) and the EUMETNET EIG GNSS water
66 vapor programme (E-GVAP, http://egvap.dmi.dk/) was established for monitoring water
67 vapor on a European scale with GNSS in near real-time for the meteorological use (Elgered
68 et al. 2005, Vedel et al. 2013). The reported quality of ZTD estimates from near real-time
69 processing are 3-10 mm (Pacione et al. 2009, Dousa and Bennitt 2013, Hadas et al. 2013).

70   Over the last decade scientific efforts were made to reduce the latency of GNSS
71 derived tropospheric products. In general, GNSS tropospheric estimates and their timely
72 provision are limited by the accuracy and latency of satellite orbit and clock products. These
73 products are critical for Precise Point Positioning (PPP) technique (Zumberge et al. 1997) that
74 is widely exploited in GNSS meteorology due to its efficiency and flexibility when analyzing
75 GNSS networks with a large number of stations (Yuan et al. 2014, Li et al 2014). The
76 majority of existing services providing ZTD for meteorology operates in near real-time, using
77 the predicted part of ultra-rapid satellite orbits and clocks. In April 2013, the International
78 GNSS Service (IGS) started Real-Time Service (RTS, http://www.igs.org/rts/), that provides
79 real-time official products for GPS and unofficial products for GLONASS (Caissy et al.
80 2012). Individual analysis centers estimate real-time products also for emerging GNSS,
81 including Galileo and BeiDou, however not all analysis centers provide open access to their
82 products.

83   The availability of precise GNSS products in real-time opened new possibilities for
84 GNSS meteorology. Dousa et al. (2013) reported standard deviation of ZTDs below 10 mm,
85 with existing systematic errors of few centimeters, attributed mainly to the incomplete
86 observation model in the software. A decrease of ZTD precision was observed for stations
87 located outside Europe and during the summer months. Ahmed et. al (2016) compared
88 several real-time ZTD estimation software packages. They noticed a significant decrease of
89 the accuracy when ignoring antenna reference point eccentricity, phase center offset and
90 variation. They also noted ZTD errors up to 4 mm when higher-order terms of ionospheric
91 delay were neglected. On the other hand, the improvement of ZTD estimation from integer
92 ambiguity fixing was at the millimeter level only. Li et al. (2015) reported a significant
93 improvement in ZTD accuracy of about several millimeters when processing multi-GNSS
94 data, rather than 10-20 mm using single system data. Dousa (2010) demonstrated that most
95 satellite orbit error could be absorbed by the satellite clock errors in PPP, so the orbit error
96 would have a limited effect on PPP derived ZTD. Shi et al. (2015) noticed a strong
97 correlation between the precision of the real-time satellite clock product and the real-time

98   GPS PPP-based ZTD solution. They recommended to choose CNES product rather than IGS
99   product in real-time. Zhu et al. (2010) investigated the effect of selection of elevation-
100 dependent weighting function and propose a cosine square model to benefit from low-
101 elevation observations. This effect was confirmed by Ning (2012), who also noticed that the
102 effect of the mapping function reduces with increasing elevation cut-off angle.

103   Although a lot of efforts have already been made to optimize real-time GNSS ZWD
104 estimation, a ZWD stochastic modeling aspect remains insufficiently investigated. In post-
105 processing it was commonly accepted to estimate ZWD as a random walk process. Dach et
106 al. (2015) suggest to impose strong relative constraints for the tropospheric parameters to
107 stabilize the system, and Kouba and Horoux (2001) recommended to assign a random walk
108 process noise (RWPN) of 5 mm/$\sqrt{h}$ for ZWD in PPP, and Pacione et al. (2009) applied a
109 ZWD constraint of 20 mm/$\sqrt{h}$. In real-time studies, Lu et al. (2015) reported a RWPN of
110 about 5-10 mm/$\sqrt{h}$, without providing further details. The majority of papers about real-time
111 ZTD or PWV estimation do not provide details about RWPN, mentioning only an epoch-wise
112 estimation of the parameter (e.g. Oliveira et al. 2016) or effective constraining based on an
113 initial empirical test (Dousa et al. 2013).

114   We investigate the sensitivity of ZWD estimates on the RWPN setting and propose
115 three methods for optimum selection of RWPN for GNSS stations located worldwide. Two
116 methods utilize historical ZWD time series from a NWP to create a global map for optimum
117 ZWD RWPN. The third method takes advantage of NWP short-term forecast to set RWPN
118 according to the expected ZWD change in NWP. We performed simulated real-time
119 processing on a representative set of globally distributed stations during summer and winter
120 seasons to validate our approach. We used official IGS ZTD products as a reference.

121   We first describe the data and products used in this study. Then we describe GNSS
122 processing methodology and methods for RWPN quantification. Thereafter, we present the
123 results of our approaches against a globally fixed RWPN, followed by the conclusions at the
124 end.

125
126

127 **Data and products**

128 This section justifies the selection of experiment time periods. It describes the GNSS data
129 processed and the reference product used in the analysis, as well as the numerical weather
130 prediction models used for RWPN estimation.

131

132   Time period

133   We selected two data periods for our experiments, each period is one week. The first period,

134   referred to below as summer campaign, is June 4-10 (DoY 155-161), 2013 and is a part of the

135   COST Action ES1206 "Advanced Global Navigation Satellite Systems tropospheric products

136   for monitoring severe weather events and climate" benchmark campaign. The second period,

137   referred to as winter campaign, is November 26 to December 2 (DoY 330-336), 2015. The

138   period selection of the winter campaign was limited due to availability of GNSS and

139   numerical weather prediction (NWP) data, and reflects opposite weather conditions to the

140   summer campaign. Both periods were chosen carefully after prior analysis of the time series

141   of IGS final ZTD for selected GNSS stations, in order to focus on challenging conditions.

142

143

144   GNSS data

145   Twenty IGS core stations distributed worldwide, in various climatic zones and in a wide

146   range of heights, were selected (Figure 1). Observations were provided in RINEX files

147   recorded with 30 second interval. Moreover, we used products of IGS RTS recorded in

148   ASCII files with Bundesamt für Kartographie und Geodäsie (BKG) Ntrip Client (BNC)

149   version 2.8 and 2.12 for the summer and winter campaigns. Although both BNC versions

150   record IGS RTS clocks and products in slightly different format, routines were developed to

151   reproduce the IGS RTS stream from both formats.

152   As reference data for our studies we used the IGS final ZTD products provided by the US

153   Naval Observatory with 5 minutes interval. The standard deviations of the final ZTDs is

154   between 1 to 2 mm, so this product is a suitable reference since the expected accuracy of the

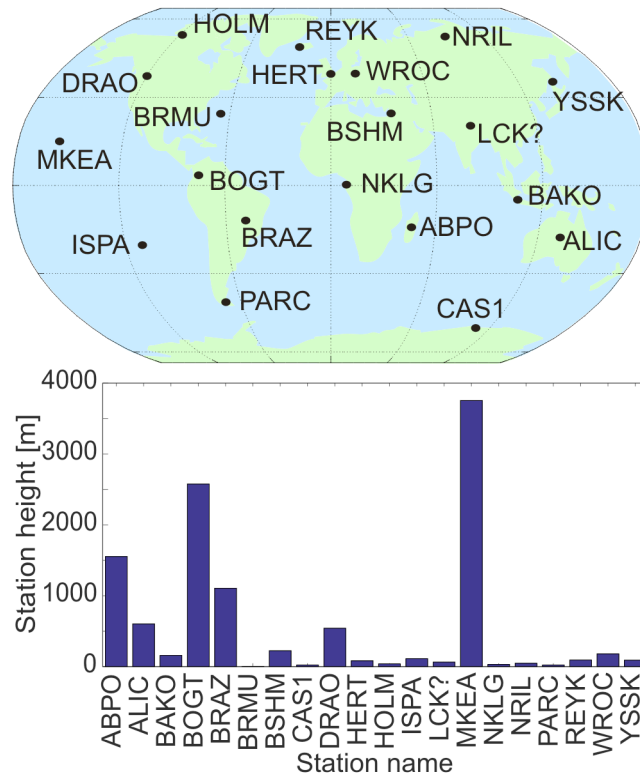155   estimated real-time ZTD is one order of magnitude larger.

Fig 1. Location (top) and heights (bottom) of GNSS test stations

Numerical Weather Models

We used data from two global NWP models, namely the European Centre for Medium-Range Weather Forecasts (ECMWF) and the National Centre for Environmental Prediction (NCEP) Global Forecast System (GFS).

The ECMWF model (http://www.ecmwf.int) provides operational forecast and re-analysis data every 6 hours and is used for the determination of hydrostatic (ZHD) and wet (ZWD) zenith delays together with the coefficients of the Vienna Mapping Functions (VMF1) in a global grid of 2.0 deg latitudinal x 2.5 deg longitudinal spatial resolution. In our study we used ZHD and ZWD directly from gridded VMF1 final products to obtain global time series for 4 years (2012 to 2015) of these two parameters, corresponding to surface values. We used ZHD and ZWD time series to estimate offline the yearly or seasonal RWPN grids.

The GFS model (http://www.emc.ncep.noaa.gov/GFS/.php) is the global forecast model of the highest temporal and spatial resolution available today. GFS4 provides forecast in 0.5 x 0.5 degree grid. Since May 2016, the GFS4 forecasts are provided hourly, but for the

175 winter campaign the forecasts were provided every three hours. For the summer campaign the
176 GFS4 was not available, so the studies with GFS4 are limited to the winter campaign only.
177 We used GFS4 short-term forecasts to reproduce ZHD and ZWD with the ray-tracing
178 technique and set RWPN dynamically in real-time processing.

179
180

181 **Methodology**

182 Using the data and products described in the previous section, we estimated RWPN from
183 NWP data and processed GNSS data in several variants. The detailed description of the
184 methodology applied in each step is provided in the following subsections.

185 GNSS data processing

186 For GNSS data processing we used the original, in-house developed GNSS-WARP software
187 (Hadas 2015) for multi-GNSS PPP. A standard PPP model is implemented in the software,
188 that includes ionospheric-free combination of pseudoranges and carrier phase measurements,
189 and ambiguities are estimated as float values. Observations are processed epoch by epoch,
190 using modified least square adjustment with propagation of the covariance matrix, which is
191 similar to a Kalman filter approach. All precise positioning correction models including
192 satellite antenna offsets, receiver antenna phase center offsets and variations, phase wind-up,
193 solid earth tides, polar tides are implemented according to IERS Convention 2010 and Kouba
194 (2015). In this study, the processing was limited to GPS data only, since only GPS is
195 officially supported by IGS RTS and many other researchers already investigated the impact
196 of multi-GNSS solution on tropospheric estimates. We adopted the strategy of the real-time
197 demonstration campaign of COST ES1206 Action: receiver coordinates were estimated as
198 static parameters, the IGS03 stream from IGS RTS was used and the parameter sampling rate
199 was 30 seconds , tropospheric gradients were not estimated. We estimated ambiguities as
200 float static values, reinitializing the ambiguity on occurrence of cycle slips. The receiver
201 clock was estimated as white noise, the elevation cut-off angle was set to 5 degrees, and we
202 applied the inverse of the sine of satellite zenith angle for observation weighting. We
203 removed the hydrostatic delay with VMF-1 derived ZHD and hydrostatic mapping function,
204 while ZWD was estimated as a random walk parameter using VMF-1 wet mapping functions.
205 Finally, we reconstruct ZTD as the sum of ZHD and ZWD at every epoch. Different ZHD
206 and ZWD estimation strategies are implemented in various software, so we will analyze

207 RWPN separately for the hydrostatic and wet components. However, in our real-time ZTD

208 estimates, we only apply wet RWPN.

209

210

211 Random Walk Process Noise

212 As already mentioned, it is commonly accepted by the GNSS community to constrain epoch-

213 wise ZWD estimates, usually by estimating ZWD as a random walk parameter. Among

214 various types of random walks, the most appropriate type for ZWD is a one-dimensional

215 Markov process (Bharucha-Reid 1960), due to its simplicity of understanding and

216 implementation. The Markov process is a memory-less stochastic process in which the future

217 value depends only on a present state, not past states (Markov property). Following the theory

218 of the Markov process, the expected translation distance S after n steps, each being of length

219 ε , is expressed by the following formula:

220
$$E(|S_n(\varepsilon)|) = \varepsilon\sqrt{n} \tag{1}$$

221 Adopting (1) to tropospheric delay ΔT and replacing the number of steps $\boldsymbol{n}$ with time t and

222 time interval δt we can write:

223
$$E(|\Delta T_{t+\delta t} - \Delta T_t|) = \varepsilon\sqrt{\delta t} \tag{2}$$

224 which means that the expected change in ΔT after the specific time interval δt depends on the

225 interval length and defined translation distance ε, which can be considered as RWPN. If we

226 know two ΔT values and the interval, we can rearrange (2) in order to estimate RWPN as:

227
$$E(\varepsilon) = |\Delta T_{t+\delta t} - \Delta T_t|/\sqrt{\delta t} \tag{3}$$

228 In case we have a time series of ΔT, we can estimate the mean RWPN as an average value

229 over the entire time series, as well as assess the uncertainty of the RWPN estimate with a

230 standard deviation for all single-epochs RWPN.

231

232

233 Ray-tracing

234 Ray-traced ZTDs are derived from 3-hourly forecasts of the GFS model using 4 model cycle

235 per day at 00, 06, 12, 18 UTC so that the most up-to-date atmospheric state is always

236 considered to minimize the forecast introduced uncertainty. The total tropospheric delay in

237 zenith direction is simply taken as an integral of refractivity N,

$$ZTD = 10^{-6} \int_{h_0}^{\infty} N(z)dz \tag{4}$$

where h_0 is a station height. The ionospheric refraction, as well as aerosols contribution to the computed delays are neglected. The atmospheric refractivity is expressed in terms of pressure P, temperature T and water vapor pressure P_w , following the separation on hydrostatic and non-hydrostatic constituents according to Davis et al. (1985),

$$N = k_1 R_d \rho + k_2' \frac{P_w}{T} + k_3 \frac{P_w}{T^2} \tag{5}$$

where k denotes "best available" empirical coefficients of refractivity given by Rüeger (2002). The new constant equals to $k_2' = k_2 - k_1 R_d/R_w$, with R_d and R_w being gas constants for dry and wet air, respectively, whereas the total mass density ρ is calculated as a sum of partial densities

$$\rho = \rho_d + \rho_w = \frac{(P-P_w)M_d}{R_u T} + \frac{P_w M_w}{R_u T} \tag{6}$$

In this equation, R_u is the universal gas constant, M_d and M_w are molar masses for dry and wet air, respectively. The vertical resolution of the GFS model is described by 26 isobaric surfaces with an uppermost level that reaches approximately 30 geopotential kilometers. Due to this limitation, a single atmospheric profile above query station coordinates is up-sampled in order to achieve vertical spacing of 10 m, 20 m, 50 m, 100 m, 500 m respectively for geometric altitudes between 0-2 km, 2-6 km, 6-16 km, 16-36 km and above 36 km as suggested by Rocken et al. (2001). Hence, the geopotential levels are converted to geometric heights to perform exponential interpolation in the domain of air pressure and water vapor pressure and linearly for temperature. The horizontal interpolation uses 2D Shepard method based on weighted mean averaging accordingly to distance from nearest model nodes. Above the upper limit of the GFS model we apply the U.S. Standard Atmosphere (1976) to provide auxiliary meteorological data up to 86 km.

Experiment variants

We used the simulated real-time mode of the GNSS-WARP software, that reconstruct real-time observation and RTS correction streams from RINEX and BNC-derived ASCII files respectively. It this way we could process the same GNSS data using 4 variants of wet RWPN settings, namely: fixed, yearly, seasonal and dynamic.

In the fixed variant we applied the same wet RWPN for all test stations. We performed 10 runs of the fixed variant, because we investigated wet RWPN in the range from

270 1 mm/√h to 10 mm/√h in steps of 1 mm/√h. The purpose of this variant was to investigate

271 whether a global optimum value for wet RWPN exists or not.

272 In the yearly variant we used (3) with ZHD and ZWD time series from VMF-1 in

273 order to estimate global grids of mean hydrostatic and wet RWPN. We estimated yearly grids

274 for each year between 2012 and 2015. For each campaign we used a grid for the year prior to

275 the processing time, to reflect the case of real-time processing. In the seasonal variant we

276 estimated time series of mean hydrostatic and wet RWPN with a 6-hour interval. We used 30-

277 day sliding window covering +/- 15 days of the corresponding time one year before the

278 current processing time. In both yearly and seasonal variants, we interpolated RWPNs for

279 each station using the 4 nearest grid points and inverse of squared distance weighting,

280 following the VMF-1 interpolation approach. The yearly variant took into account the global

281 variability of RWPN, while the seasonal variant also took into account the variability over

282 seasons. The reason why we also calculated hydrostatic RWPN grids is related to the

283 different tropospheric estimation strategies that might be implemented in other software. In

284 case ZTD, not ZWD, is estimated directly, the ZTD RWPN can be calculated as a root square

285 of the sum of squared hydrostatic and wet RWPNs.

286 In the dynamic variant we took advantage of the GFS4 model and ray-tracing

287 technique. Every 3 hours we estimated new wet RWPNs using (3) and two consecutive

288 epochs of the shortest available GFS4 forecasts. This variant is similar to the seasonal variant,

289 as it also takes into account the temporal variability of RWPN. The advantage is the use of

290 current rather than historical data, and a two times higher temporal resolution. Although this

291 variant is the only one that requires additional computational power to perform ray-tracing, it

292 was already shown by Zus et al. (2014) and Wilgan (2015) that the delivery of NWP-

293 troposphere products in real-time is possible.

294

295

296 **Results**

297 We analyzed the processing results paying particular attention to RWPN differences among

298 experiment variants and compared ZTD estimates with the reference product to verify the

299 proposed methods of RWPN quantification.

300

301 Hydrostatic and wet RWPN grids

302 Yearly mean hydrostatic and wet RWPN grids are presented in Figure 2. We noticed both
303 hydrostatic and wet RWPN to be geographically dependent. Hydrostatic RWPN varies from
304 0.3 mm/√h around poles to 4.1 mm/√h for ocean areas along 60°S latitude. The mean
305 hydrostatic RWPN value is 1.8 mm/√h with a standard deviation of 0.7 mm/√h. In all
306 hydrostatic grids we noticed an occurrence of regular cycles along the equator, shifted by 90
307 degrees. This corresponds to the temporal resolution of the ECMWF model. Although the
308 hydrostatic RWPN differences along the tropical region are smaller than 1mm/√h, this
309 reveals a drawback of the approach. Wet RWPN varies from 0.1 mm/√h over Antarctica and
310 Greenland to 12.0 mm/√h over some ocean areas along 40°N and 40°S latitude. The mean
311 wet RWPN value is 5.0 mm/√h with a standard deviation of 2.8 mm/√h. Please note that wet
312 RWPN values estimated with (3) and NWP data correspond well to the constraining applied
313 by various researchers, already mentioned above. This confirms that the strategy of wet
314 RWPN estimation based on Markov process theory is suitable for real-time GNSS ZTD
315 estimation.

316 We noticed that grids are nearly identical year by year, with differences below
317 1mm/√h for hydrostatic and wet grids. This means that a single RWPN grid can be
318 implemented in a software in case only one static RWPN value per station is acceptable,
319 without significant degradation of the grid accuracy. For further processing in the yearly
320 variant we used 2012 grids for the summer campaign and 2014 grids for the winter campaign,
321 taking into account that those grids would have been available in case of real-time
322 processing.
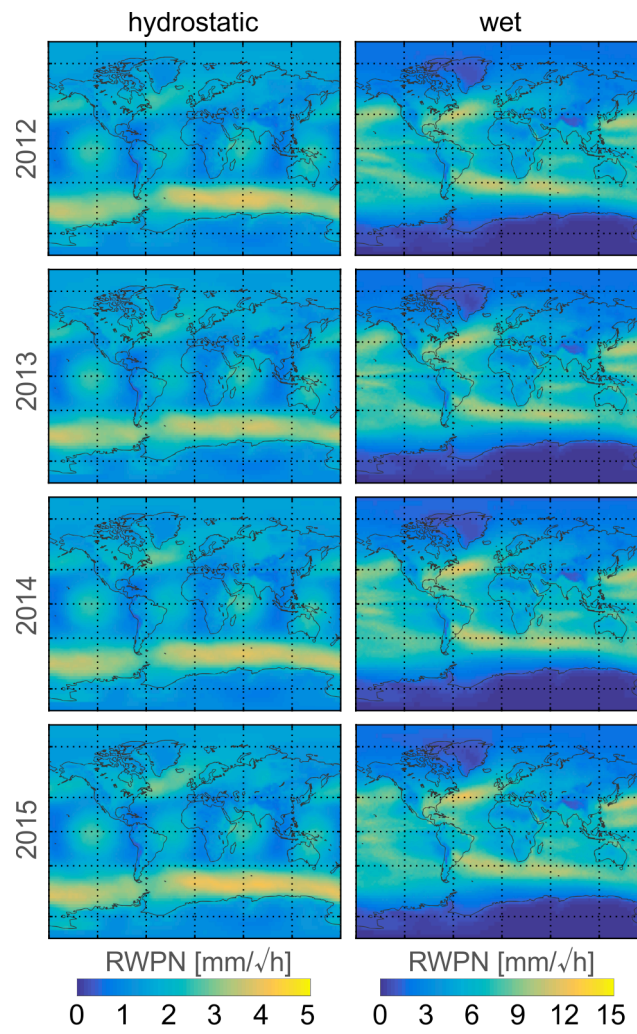
Fig. 2 Hydrostatic (top) and wet (bottom) yearly mean RWPN grids over 2012-2015
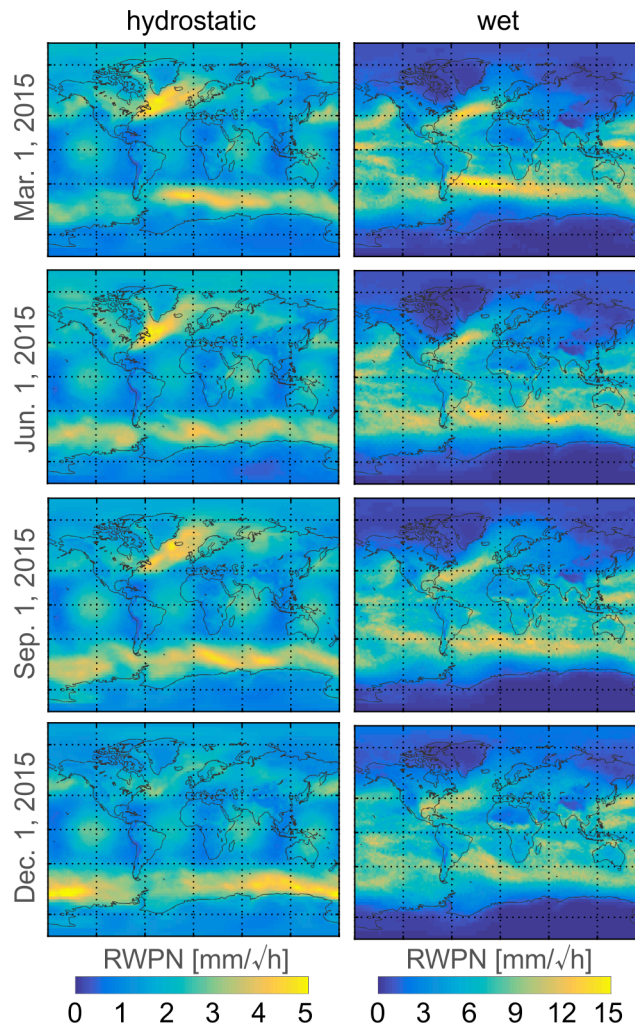
Fig. 3 Hydrostatic (top) and wet (bottom) seasonal mean RWPN grids for 4 different seasons in 2015

Seasonal mean RWPN grids are presented in Figure 3. For clarity, we present only 4 grids from 2015, each grid shifted in time by 3 months, in order to present different seasons. Hydrostatic RWPN varies from 0.1 mm/√h around poles to 5.4 mm/√h for ocean areas along 60°S latitude and the northern part of the North Atlantic Ocean. The mean hydrostatic RWPN value is 1.8 mm/√h with a standard deviation of 0.8 mm/√h. Wet RWPN varies from 0.1 mm/√h over Antarctica and Greenland to 16.4 mm/√h over some ocean areas along 40°N and 40°S latitude. The mean wet RWPN value is 4.8 mm/√h with a standard deviation of 3.2 mm/√h.

We noticed that both hydrostatic and wet RWPN vary not only geographically but also seasonally. The seasonal hydrostatic RWPN differences reach 2.9 mm/√h over the north part of the North Atlantic Ocean, and 1.7 mm/√h over the south part of the South Atlantic Ocean. The seasonal wet RWPN differences reach 7.3 mm/√h over the South Atlantic Ocean

342 along 40ºS latitude, 4.8 mm/√h between 45ºN and 45ºS and 2.0 mm for the remaining areas.

343 The wet RWPN differences are significantly larger over ocean areas than over the continents.

344

345

346 Case studies

347 We investigated real-time ZTD estimates among variants for each station individually. We

348 applied the simple ZTD quality filter by setting the threshold of 10 mm for the ZTD formal

349 error in order to remove outliers and estimates during the solution initialization period. The

350 best fixed variant was selected following the criteria of the smallest standard deviation of

351 residuals between real-time and final solutions, while the percent of epochs with sufficient

352 solution quality remains high. We found that the larger wet RWPN, the lower is the

353 availability of the solution. We noticed a station specific bias between real-time and final

354 solutions, that is a well-known case in GNSS meteorology. Fortunately, for meteorological

355 applications it can be corrected with monthly mean (Bennit and Jupp 2012, Dousa et al.

356 2013). Moreover, this bias differs by less than 0.1 mm among all real-time variants, so it will

357 not be a subject of further analysis. In general, we found two groups of stations: 1) in which

358 yearly and seasonal variants are almost as good as the best fixed variant, while the dynamic

359 variant is as good as or even better than the best fixed variant, 2) in which the results are

360 ambiguous. Fortunately, only 6 from 20 stations can be assigned to the second group,

361 namely: HOLM and NRIL (in the summer campaign only), BRAZ (in the winter campaign

362 only), ABPO, ISPA and YSSK (in both campaigns).

363   A representative station in group 1) is station HERT (Figure 4). In general, time series

364 of estimated ZTD among variants fits well to the final solution. The best fixed solution is

365 obtained for wet RWPN=4 mm/√h in the summer campaign and wet RWPN=7 mm/√h in the

366 winter campaign. In both campaigns yearly and seasonal wet RWPNs differ less than

367 1mm/√h over the test periods, therefore both variants result in very similar ZTD estimates.

368 Both variants result in equally precise ZTD estimates as in the best fixed variant. The

369 availability of solutions is also equally high, except for the seasonal variant in the winter

370 campaign, when the availability is lower by 0.2%. An improvement in real-time ZTD quality

371 is obtained for the dynamic variant, that reduces standard deviation of ZTD residuals by 18%,

372 keeping high availability of the accepted estimates. The improvement in real-time ZTD is

373 significant in case of dynamic changes of tropospheric conditions e.g. late evening of DoY

374 331, around noon of DoY 334 and 335, and evening of DoY 336 in 2015. In these periods,

the dynamic wet RWPN setting is high, thus allowing the PPP filter to change the ZWD estimates rapidly. For the remaining periods, the dynamic RWPN is lower, so that ZWD estimates remain more stable over time, e.g. during DoY 330 and from the evening of DoY 335 to the evening of DoY 336 in 2015.
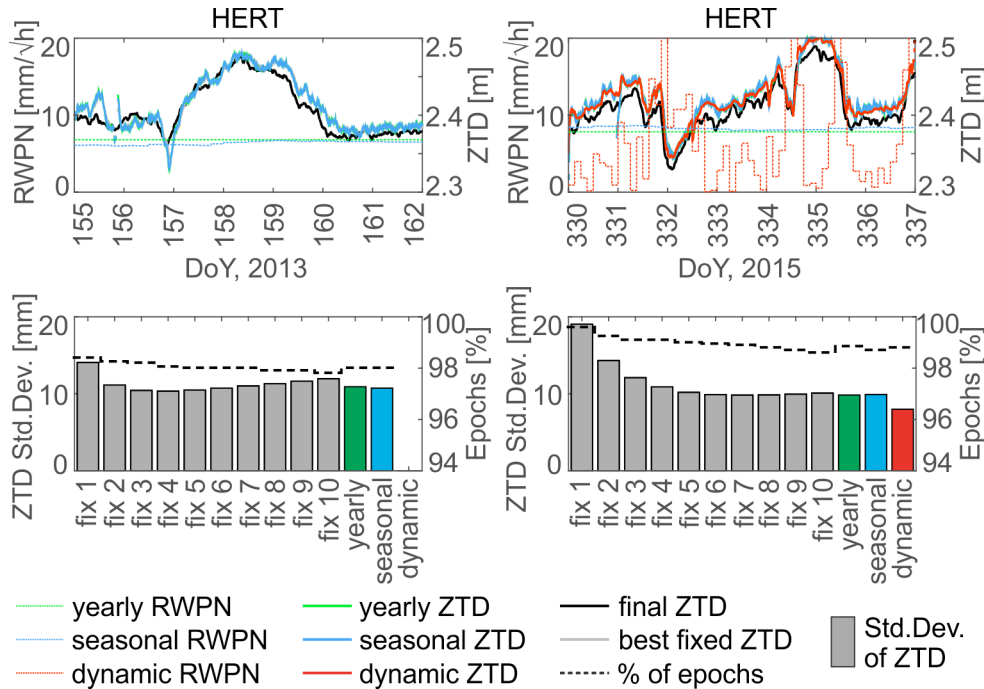
Fig. 4 Comparison of wet RWPN, ZTD time series, standard deviations of real-time ZTD residuals with respect to the final ZTD and solution availability among variants for station HERT

384
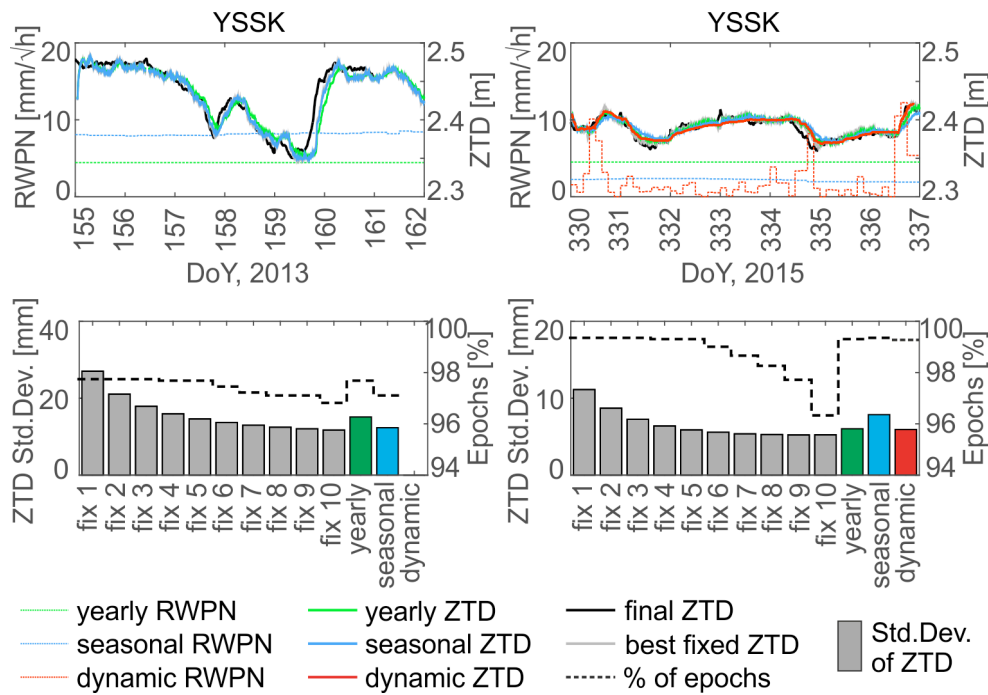
Fig. 5 Comparison of wet RWPN, ZTD time series, standard deviations of real-time ZTD
residuals with respect to the final ZTD and solution availability among variants for station
YSSK

Station YSSK (Figure 5) is a representative example of stations from the group 2). In
this case it is impossible to unambiguously indicate the best fixed wet RWPN, because the
larger the RWPN, the smaller is the standard deviation; for RWPN larger than 5 mm/√h, we
observe a significant reduction of solution availability. A subjective selection of the best
fixed variant will be RWPN=5 mm/√h both for summer and winter campaign, as it keeps the
high percentage of available solutions while the improvement in ZTD quality is not so
significant for larger RWPN settings. The yearly variant returns very similar results to the
best fixed variant in both campaigns. The seasonal wet RWPN differs significantly from the
yearly wet RWPN in both campaigns, therefore the quality and availability of the results vary
among campaigns and do not correspond to the best fixed solution. The dynamic variant
returns results that are comparable with the yearly approach, in the sense of low standard
deviation of residuals and high availability of results. However, the time series of yearly and
dynamic variant varies. The dynamic time series is much smoother due to very low dynamic
RWPN setting for most of the time.

404

405   Comparison against global RWPN

406   We compared best fixed, yearly, mean seasonal and mean dynamic wet RWPN values, as

407   well as the availability and quality of estimated ZTD among stations for both campaigns. The

408   comparison of wet RWPN among variants is presented in Figure 6. For the best fixed RWPN

409   value, the differences between campaigns are usually about 2-3 mm/√h. The yearly RWPN

410   often agreed with the best fixed RWPN at the level of 2 mm/√h, but for some stations the

411   disagreement is strong, e.g. stations BOGT, LCK4, NRIL, and YSSK. The seasonal RWPN

412   differs from the corresponding yearly RWPN also by a few mm/√h, and the differences in

413   seasonal RWPN between campaigns range from 0 mm/√h to 5.8 mm/√h. The mean dynamic

414   RWPN usually corresponds well to the yearly RWPN, with differences from 0 to 3 mm/√h.

415   The RWPN in all variants varies significantly among stations, and we did not find any

416   relation between the best fixed wet RWPN value and station location or its height. It means

417   that, as expected, the best wet RWPN value is both location and time specific because it

418   depends on the atmospheric conditions.
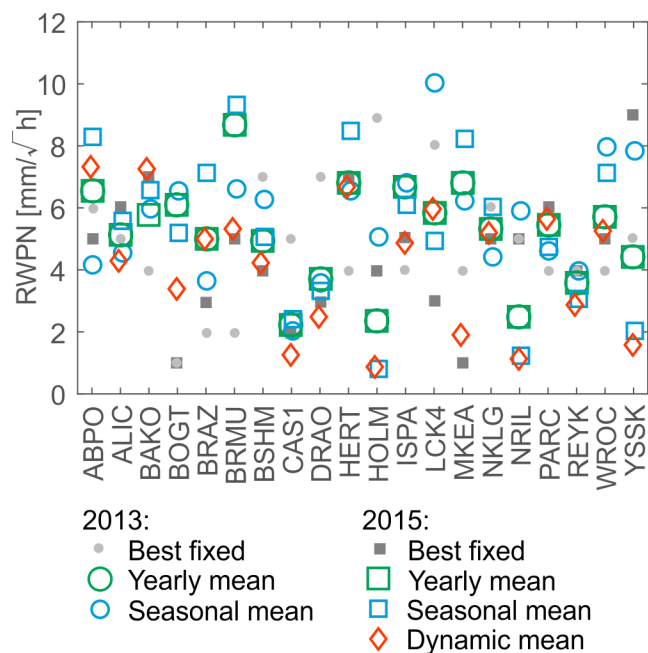
419

420   **Fig. 6** Comparison of wet RWPN among variants and campaigns

421

422   We also compared variants in the sense of availability of accepted ZWD estimates

423   (Figure 7). We found that availability is over 95% for 17 stations in the summer campaign

424   (the worst stations are BOGT, LCK4 and MKEA) and 19 stations in the winter campaign (the

425 worst station is MKEA). Again, we noticed the decrease of availability with an increase of
426 wet RWPN in the fixed variant. The yearly variant provides similar ZWD estimates
427 availability if RWPN=6 mm/√h in the summer campaign and RWPN=7 mm/√h in the winter
428 campaign are applied to all stations. The seasonal approach is, in general, slightly worse than
429 the yearly approach. In the dynamic variant, the availability for station MKEA increased
430 significantly to 76%, compared to 38% in the yearly variant. For few stations the availability
431 is slightly decreased, by less than 2% compared with the yearly variant.

432 We also compared variants in the sense of the quality of estimated real-time ZTD, by
433 analyzing the standard deviation of ZTD residuals with respect to the ZTD final estimates
434 (Figure 8). We found the best empirical global value of wet RWPN is 8 mm/√h in the
435 summer campaign and 6 mm/√h in the winter campaign. In the summer campaign, for fixed
436 wet RWPN > 5 mm/√h, as well as in the yearly and seasonal variants, the average standard
437 deviation is around 10 mm, and does not exceed 20 mm for any station. Compared to the best
438 fixed variant, the yearly and seasonal variants resulted in a slightly higher and slightly lower
439 standard deviation, respectively. In the winter campaign for global wet RWPN=6 mm/√h, the
440 standard deviation of residuals varies from 3.8 mm to 16.8 mm with a mean value of 9.7 mm.
441 The yearly variant resulted in a slightly lower standard deviation compared to the best fixed
442 variant, while the seasonal variant resulted in a higher standard deviation than both the yearly
443 and best fixed variants. The dynamic variant significantly improves the accuracy, the
444 standard deviation of residuals varies from 4.2 mm to 14.7mm with a mean value of 9.2 mm.

445

DoY 155-161, 2013

DoY 330-336, 2015
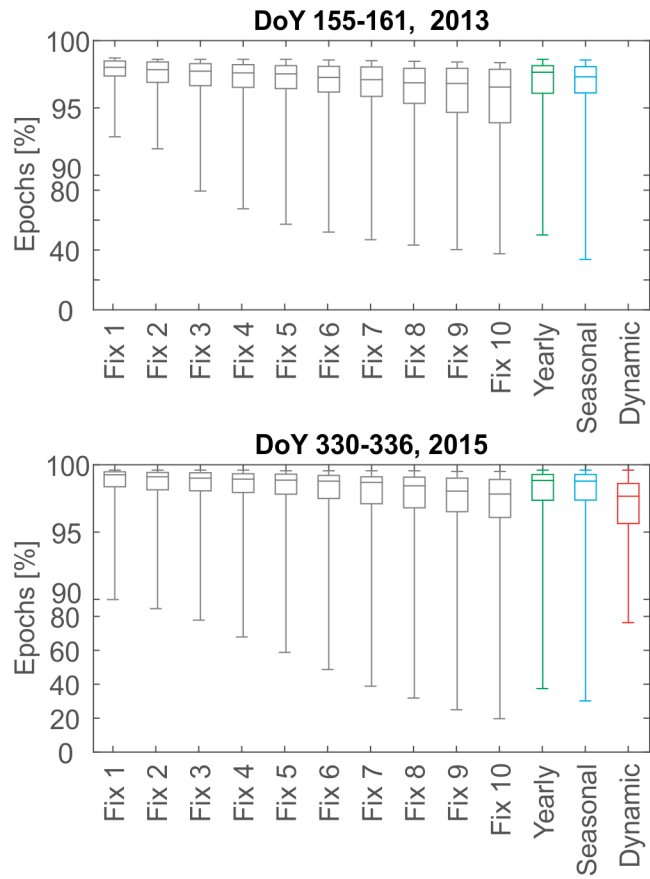
446

447   **Fig. 7** Availability of epochs with estimated real-time ZTD. Note different scales of the

448   vertical axis between ranges 0-90% and 90-100 %
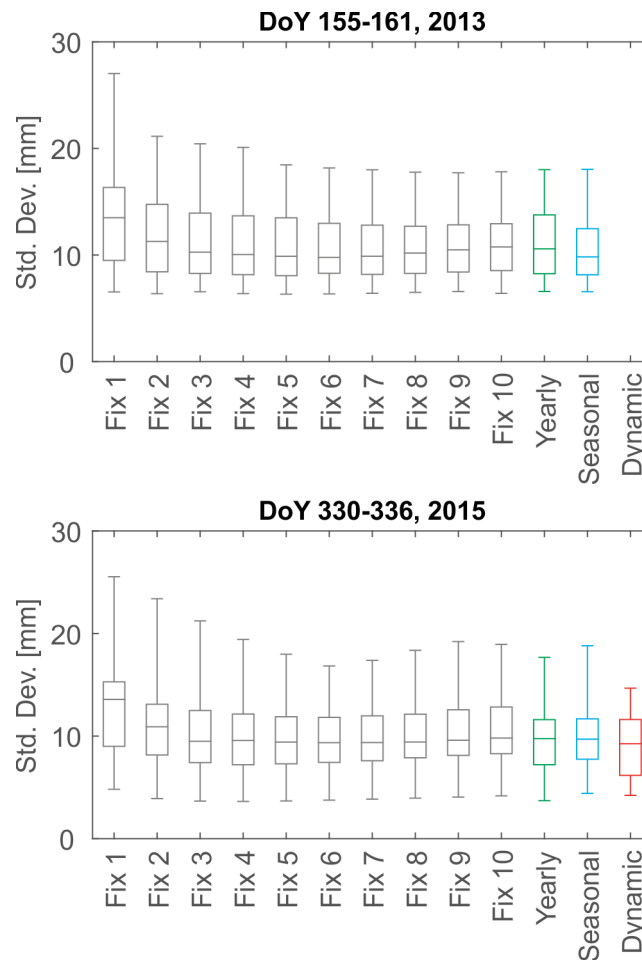
449

Fig. 8 Standard deviation of real-time ZTD residuals with respect to the final ZTD

Comparison against station-specific RWPN

Finally, we checked if any of the proposed variants can provide results of the same quality as if the fixed RWPN is adjusted empirically for each station and each campaign individually. The results for the summer and winter campaign are presented in Tables 1 and 2, respectively. The results presented in the individually fixed row correspond to the case when an initial empirical test is performed for each station individually. These results should be considered as target values, because better results cannot be obtained with any other fixed RWPN value. If any of the proposed variants can eliminate the requirement of an initial empirical test, the results should be close to the target values. It is important to note, that it is not possible to perform such an ideal empirical test in real-time processing, because RWPN can only be empirically adjusted to a past time series, so it may not be suitable for the current atmospheric conditions.

466   We found that the yearly variant is, in general, only slightly worse than the empirical
467 testing, providing very similar availability of data, while the standard deviation of residuals is
468 larger by 0.8 mm both in the summer and winter campaigns. There is only one station,
469 namely MKEA, for which the results in the winter campaign are degraded (from 14.2 mm to
470 17.7 mm) and of lower availability (by 51%). For the seasonal variant, the availability of
471 solution is lower than in the yearly variant, and the accuracy is comparable or even worse
472 than in the yearly variant. The dynamic variant provides significantly better results than the
473 yearly variant, increasing the availability of results on average from 95.2% to 96.9% and
474 reducing the average standard deviation from 9.7 mm to 9.2 mm.

475

476   **Table 1** Wet RWPN range, available epochs and standard deviations among processing
477   variants, DoY 155-161, 2013

	RWPN [mm/$\sqrt{h}$]		Epochs [%]			StdDev [mm]		
	Min	Max	Avg	Min	Max	Avg	Min	Max
Indiv. fixed	2.0	9.0	93.7	60.7	98.2	10.3	6.3	17.4
Yearly	2.2	8.6	93.4	60.7	98.3	11.1	6.6	18.0
Seasonal	1.8	11.2	92.5	41.0	98.2	10.9	6.6	18.0

478

479   **Table 2** Wet RWPN range, available epochs and standard deviations among processing
480   variants, DoY 330-336, 2015

	RWPN [mm/$\sqrt{h}$]		Epochs [%]			StdDev [mm]		
	Min	Max	Avg	Min	Max	Avg	Min	Max
Indiv. fixed	1.0	9.0	97.5	87.7	99.5	8.9	3.6	14.2
Yearly	2.2	9.3	95.2	36.4	99.5	9.7	3.7	17.7
Seasonal	0.8	10.1	94.8	30.4	99.5	9.8	4.4	18.8
Dynamic	0.0	45.3	96.9	73.2	99.5	9.2	4.2	14.7

481
482

483

Conclusions

We have shown that the optimum ZWD constraints in real-time GNSS processing, modelled as a random-walk process, should be time and location specific. This means that a single random walk processing noise (RWPN) value should not be applied globally to all stations, because it may lead to significant degradation of solution quality. We performed empirical tests for each station and each campaign individually in order to get reference values of wet RWPN, for which the standard deviation with respect to the final ZTD estimates is low, and the availability of the real-time solution is high. It is important to note, that empirical testing was performed in post-processing mode, so wet RWPN values were adjusted to the current set of data, which is not the case in real-time processing.

In order to eliminate prior empirical testing, we propose 3 strategies to estimate RWPN that use Gauss-Markov process theory and NWP data of limited temporal and spatial resolution. We compared the quality of the results obtained with the proposed strategies against the results obtained with the empirical testing. In general, this comparison showed, that with yearly wet RWPN grids we can reconstruct, with a mean error of 1mm/√h, the wet RWPN value obtained from empirical testing. Because yearly grids are very similar year by year, it is sufficient to implement only a single yearly grid in a software as a look up table to define the optimum wet RWPN value for any station located worldwide. However, it is recommended to make an update every few years. Such a grid is a novelty product for the GNSS community that eliminates the time-consuming and period-sensitive empirical testing. A further improvement is foreseen in an ECMWF replacement with a NWP model of higher spatial and temporal resolution, which is a goal of our future studies. Moreover, a longer time period should be investigated in order to determine how often (if at all) such a grid should be updated.

The seasonal wet RWPN grids lead to slightly worse results than the yearly grids. Therefore, and due to the increased complexity of seasonal grid implementation, this strategy is not recommended. The degradation of the real-time ZTD quality in the seasonal variant can be explained by the incorrect assumption that seasonal tropospheric conditions repeat every year.

A superior result was obtained with the third proposed strategy, namely the dynamic strategy, which is based on regular ray-tracing through a shortest available forecast from a NWP model. The results are almost as good as those from the post-processing empirical testing.

516 The advantage of this approach is that the wet RWPN is regularly adjusted to the current

517 tropospheric conditions. Its value remains low, when ZTD is stable over time, and rises when

518 a rapid change of ZTD is expected. The drawback of this approach is high computational

519 power required to perform NWP ray-tracing on a regular basis for each station in the

520 processing. It should be verified in the near future, if a NWP model of higher spatial and

521 temporal resolution can further improve real-time ZTD estimates.

522

523

533

534

535 **References**

536 Ahmed F, Vaclavovic P, Teferle FN, Dousa J, Bingley R, Laurichesse D (2016) Comparative

537 analysis of real-time precise point positioning zenith total delay estimates. GPS Sol

538 20:187:199. doi: 10.1007/s10291-014-0427-z

539

540 Bennitt GV, Jupp A (2012) Operational Assimilation of GPS Zenith Total Delay

541 Observations into the Met Office Numerical Weather Prediction Models. Mon Weather Rev

542 140(8):2706-2719

543

544 Bevis M, Businger S, Chiswell S, Herring TA, Anthes RA, Rocken C, Ware RH (1992) GPS

545 meteorology: remote sensing of atmospheric water vapor using the global positioning system.

546 J Geophys Res 97(D14):15787–15801

547

548   Bianchi CE, Mendoza LPO, Fernandez LI, Moitano JF (2016) Multi-year GNSS monitoring

549   of atmospheric IWV over Central and South America for climate studies. Ann Geo

550   34(7):623-639. doi: 10.5194/angeo-34-623-2016

551

552   Böhm J, Kouba J, Schuh H (2009) Forecast Vienna Mapping Functions 1 for real-time

553   analysis of space geodetic observations. J Geod 86(5):397-401

554

555   Bharucha-Reid AT (1960) Elements of the Theory of Markov Processes and Their

556   Applications. New York: McGraw-Hill

557

558   Caissy M, Agrotis L, Weber G, Hernandez-Pajares M, Hugentobler U (2012) Coming soon:

559   The International GNSS Real-Time Service. GPS World 23(6):52–58

560

561   Dach R, Lutz S, Walser P, Fridez P (2015) Bernese GNSS Software Version 5.2. User

562   manual, Astronomical Institute, University of Bern, Bern Open Publishing. doi:

563   10.7892/boris.72297; ISBN: 978-3-906813-05-9

564

565   Davis JL, Herring TA, Shapiro II, Rogers AEE, Elgered G (1985) Geodesy by radio

566   interferometry: Effects of atmospheric modeling errors on estimates of baseline length, Radio

567   Sci., *20(6),* 1593–1607.

568

569   Dousa J (2010) Precise near real-time GNSS analyses at Geodetic observatory Pecný -

570   precise orbit determination and water vapor monitoring. Acta Geodyn Geomater 7(1):1-11

571

572   Dousa J, Bennitt GV (2013) Estimation and evaluation of hourly updated global GPS Zenith

573   Total Delays over ten months. GPS Sol 17:453:464

574

575   Dousa J, Vaclavovic P, Gyori G, Kostelecky J (2013) Development of real-time GNSS ZTD

576   products. Adv Space Res 53:1347-1358

577

578   Elgered G, Plag HP, Van der Marel H, Barlag S, Nash J (2005) COST action 716 -

579   exploitation of ground-based GPS for operational numerical weather prediction and climate

580   applications. Official Publications of the European Communities, Luxembourg

581

582 Guerova G, Jones J, Dousa J, Dick G, De Haan S, Pottiaux E, Bock O, Pacione R, Elgered G,

583 Vedel H, Bender M (2016) Review of the state-of-the-art and future prospects of the ground-

584 based GNSS meteorology in Europe. Atmos Meas Tech Discuss. doi: 10.5194/amt-2016-125

585

586 Hadas T (2015) GNSS-Warp Software for Real-Time Precise Point Positioning. Artif

587 Satellites, 50(2):59-76

588

589 Hadas T, Kaplon J, Bosy J, Sierny J, Wilgan K (2013) Near-real-time regional troposphere

590 models for the GNSS precise point positioning technique. Meas Sci Technol 24(5):055003-

591 055014

592

593 Hernández-Pajares M, Juan JM, Sanz J, Colombo OL, Van der Marel H (2001) A new

594 strategy for real-time integrated water vapor determination in WADGPS Networks. Geophys

595 Res Lett 28(17):3267-3270

596

597 Hopfield HS (1969) Two-quartic tropospheric refractivity profile for correcting satellite data.

598 J Geophys Res 74:4487–4499

599

600 Karabatic A, Weber R, Haiden T (2011) Near real-time estimation of tropospheric water

601 vapor content from ground based GNSS data and its potential contribution to weather now-

602 casting in Austria. Adv Space Res 47:1691–1703

603

604 Kouba J (2015) A guide to Using the IGS Products. Online: http://kb.igs.org/hc/en-

605 us/articles/201271873-A-Guide-to-Using-the-IGS-Products (access 17.08.2016)

606

607 Kouba J, Heroux P (2001) Precise Point Positioning Using IGS Orbit and Clock Products.

608 GPS Sol 5(2):12-28

609

610 Lagler K, Schindelegger M, Böhm J, Krásná H, Nilsson T (2013) GPT2: Empirical slant

611 delay model for radio space geodetic techniques. Geophys Res Lett 40:1069–1073. doi:

612 10.1002/grl.50288.

613

614   Leandro RF, Santos MC, Langley RB (2006) UNB neutral atmosphere models: development
615   and performance. Proc ION NTM 2006, Institute of Navigation, Monterey, CA, January 18–
616   20, 564–573

617

618   Li X, Dick G, Ge M, Heise S, Wickert J, Bender M (2014) Real-time GPS sensing of
619   atmospheric water vapor: Precise point positioning with orbit, clock and phase delay
620   corrections. Geophys Res Lett 41(10):3615-3621. doi: 10.1002/2013GL058721

621

622   Li X, Dick G, Lu C, Ge M, Nilsson T, Ning T, Wickert J, Schuh H (2015) Multi-GNSS
623   Meteorology: Real-Time Retrieving of Atmospheric Water Vapor From BeiDou, Galileo,
624   GLONASS, and GPS Observations. IEEE Transactions On Geoscience And Remote Sensing.
625   doi: 10.1109/TGRS.2015.2438395

626

627   Lu C, Li X, Nilson T, Ning T, Heinkelmann R, Ge M, Glaser S, Schuh H (2015): Real-time
628   retrieval of precipitable water vapor from GPS and BeiDou observations. J Geod 89(9): 843-
629   856

630

631   Mendes VB (1999) Modeling the neutral-atmospheric propagation delay in radiometric space
632   techiniques. PhD dissertation, University of New Brunswick

633

634   Niell AE (1996) Global mapping functions for the atmosphere delay at radio wavelengths. J
635   Geophys Res 101:3227–46

636

637   Ning T (2012) GPS meteorology: with focus on climate applications. PhD thesis, Chalmers
638   University of Technology, ISBN 978-91-7385-675-1

639

640   de Oliveira PS, Morel L, Fund F, Legros R, Monico JFG, Durand S, Durand F (2016)
641   Modeling tropospheric wet delays with dense and sparse network configurations for PPP-
642   RTK. GPS Sol (online). doi: 10.1007/s10291-016-0518-0

643

644   Pacione R, Vespe F (2008) Comparative studies for the assessment of the quality of near-
645   real-time GPS-derived atmospheric parameters. J Atmos Ocean Tech 25:701–714

646

647   Pacione R, Vespe F, Pace B (2009) Near Real-Time GPS Zenith Total Delay validation at E-

648   GVAP Super Sites. Bollettino Di Geodesia E Scienze Affini 1

649

650   Rocken C, Sokolovskiy S, Johnson JM, Hunt D (2001) Improved mapping of tropospheric

651   delays. J Atmos Oceanic Tech, 18(7), 1205-1213.

652

653   Rohm W, Yang Y, Biadeglgne B, Zhang K, Le Marshall J (2014) Ground-based GNSS

654   ZTD/IWV estimation system for numerical weather prediction in challenging weather

655   conditions. Atmos Res 138:414-426. doi: 10.1016/j.atmosres.2013.11.026

656

657   Rüeger JM (2002) Refractive index formulae for radio waves. Integration of techniques and

658   corrections to achieve accurate engineering. Proc XXII FIG International Congress,

659   Washington, DC, USA, April 19–26, 1-13

660

661   Saastamoinen J (1972) Contributions to the theory of atmospheric refraction. Bull Géod

662   105:13–34

663

664   Satirapod C, Anonglekha S, Coy Y, Lee H (2011) Performance assessment of GPS-sensed

665   precipitable water vapor using IGS ultra-rapid orbits: a preliminary study in Thailand. Eng J

666   15:1-8

667

668   Shi J, Xu C, Li Y, Gao Y (2015) Impacts of real-time satellite clock errors on GPS precise

669   point positioning-based troposphere zenith delay estimation. J Geod 89:747-756

670

671   US Standard Atmosphere (1976) NASA TM-X 74335. National Oceanic and Atmospheric

672   Administration. National Aeronautics and Space Administration and United States Air Force

673   Vedel H, De Haan S, Jones J, Bennitt G, Offiler D (2013) E-GVAP third phase. Geophys Res

674   Abstracts 15: EGU2013-10919

675

676   Vedel H, Mogensen K, Huang XY (2001) Calculation of Zenith Delays From Meteorological

677   Data Comparison of NWP Model, Radiosonde and GPS Delays. Phys Chem Earth 26:497–

678   502. doi: 10.1016/S1464-1895(01)00091-6

679

680   Wilgan (2015) Zenith total delay short-term statistical forecasts for GNSS Precise Point

681   Positioning. Acta geodyn geometer 12(4):335-343

682

683   Yuan Y, Zhang K, Rohm W, Choy S, Norman R, Wang SC (2014) Real-time retrieval of

684   precipitable water vapor from GPS precise point positioning. J Geophys Res Atmos

685   119(6):10044-10057. doi: 10.1002/2014JD021486

686

687   Zhu Q, Zhao Z, Lin L, Wu Z (2010) Accuracy Improvement of Zenith Tropospheric Delay

688   Estimation Based on GPS Precise Point Positioning Algorithm. Geo Spat Inf Sci 13(4):306-

689   310

690   Zumberge JF, Heflin MB, Jefferson DC, Watkins MM Webb FH (1997) Precise Point

691   Positioning for the Efficient and Robust Analysis of GPS Data from Large Networks. J

692   Geophys Res 102(B3):5005-5018. doi:10.1029/96JB03860

693

694   Zus F, Dick G, Dousa J, Heise S, Wickert J (2014) The rapid and precise computation of GPS

695   slant total delays and mapping factors utilizing a numerical weather model. Radio Sci

696   49(3):207–216

697

Tomasz Hadas received his PhD in satellite geodesy in 2015. He is an assistant professor at the Institute of Geodesy and Geoinformatics, Wroclaw University of Environmental and Life Sciences, Poland. He is working on development of GNSS real-time precise positioning algorithms, troposphere modelling in real-time and application of atmosphere models into GNSS positioning.

705

706

707

708

709

Felix Norman Teferle is Professor of Geodesy at the University of Luxembourg, Luxembourg. His research focuses on improving GNSS processing strategies and bias models for high-precision positioning while applying the technique to a range of geodetic and geophysical problems. Particular areas of interest are the monitoring of land movements in relation to sea level studies, the estimation of atmospheric water vapor and the stochastic modelling of time series.

716

717

718

719

720

Kamil Kazmierski graduated from Wroclaw University of Environmental and Life Sciences in 2014 obtaining a Master Degree in Geodesy and Cartography. He is a PhD student at the Institute of Geodesy and Geoinformatics, Wroclaw University of Environmental and Life Sciences, Poland. He is working on development of Multi-GNSS real-time precise positioning algorithms.

727

728

729

730

731

732

Pawel Hordyniec graduated from Wroclaw University of Environmental and Life Sciences in 2013 with a Master Degree in Geodesy and Cartography. He is a PhD student and a research assistant at the Institute of Geodesy and Geoinformatics, Wroclaw University of Environmental and Life Sciences, Poland. His main field of research is GPS radio occultation technique and signal ray-tracing for ground- and space-based GNSS applications.

740

741

742

743

744

Jaroslaw Bosy has been a Professor at the Institute of Geodesy and Geoinformatics, Wroclaw University of Environmental and Life Sciences, Poland since 2008. He was awarded a PhD in Geodesy and Cartography in 1996 and habilitation in 2006 from Faculty of Mining Surveying and Environmental Engineering of AGH University of Science and Technology, Krakow, Poland. His research are concentrated on reference frames realization in global, regional and local scale using GNSS techniques to derive information about the state of the atmosphere and application of GNSS technique in geodesy and geodynamics.

752

753